Population Ecology (2018) 60:37–47
https://doi.org/10.1007/s10144-018-0619-4

THE SOCIETY OF POPULATION ECOLOGY

SPECIAL FEATURE: ORIGINAL ARTICLE

Evolutionary demography: the dynamic and broad intersection of ecology and evolution

A cautionary note on elasticity analyses in a ternary plot using randomly generated population matrices

Takenori Takada[1] · **Yuka Kawai**[1] · **Roberto Salguero-Gómez**[2,3,4,5]

Received: 7 September 2017 / Accepted: 7 May 2018 / Published online: 23 May 2018

Abstract

Matrix population models are one of the most common mathematical models in ecology, which describe the dynamics of stage-structured populations and provide us many population statistics. One of the statistics, elasticity onto population growth rate, is frequently used and represents the degree of the relative impact of life history parameters to the population growth rate. Due to the utility of elasticities for cross-taxonomic comparisons, Silvertown and his coauthors have published multiple papers and reported the relationship between elasticities and life forms (or life history) in multiple plant species, using a triangle map (called "ternary plot"). To understand why their elasticities are located in specific regions of the ternary plot, we constructed four archetypes of population matrices, from which we simulated 24,000 randomly generated population matrices and obtained the consequent elasticities. We found a large discrepancy when comparing our results to those in Silvertown et al.'s study (Conserv Biol 10:591–597, 1996): for our simulated matrices where rapid transitions were not allowed (e.g., trees), the elasticity distribution resulted in a line across the ternary plot. We provided the mathematical proof for this result, and found that its slope depends on matrix dimension. We also used 1230 matrices from the COMPADRE Plant Matrix Database and calculated the elasticities. Our simulated results were validated with field data from COMPADRE: two straight lines appeared in the ternary plot. Furthermore, we answered several addressed questions, such as, "Is there any special elasticity distribution in matrices with high population growth rates?" and "Why are the elasticities of natural populations concentrated in the upper half of the ternary plot?".

Keywords COMPADRE plant matrix database · Comparative biology · Demographic simulation · Elasticity vector distribution · Population matrix models

Electronic supplementary material The online version of this article (https://doi.org/10.1007/s10144-018-0619-4) contains supplementary material, which is available to authorized users.

✉ Takenori Takada
takada@ees.hokudai.ac.jp

[1] Graduate School of Environmental Science, Hokkaido University, Kita-ku, Sapporo 060-0810, Japan

[2] Department of Zoology, Oxford University, New Radcliffe House, Radcliffe Observatory Quarter, 6GG, Woodstock Rd, Oxford OX2, UK

[3] Centre for Biodiversity and Conservation Science, University of Queensland, St. Lucia, QLD 4071, Australia

[4] Evolutionary Demography Laboratory, Max Plank Institute for Demographic Research, 18057 Rostock, Germany

[5] Department of Animal and Plant Sciences, University of Sheffield, Alfred Denny Building, Western Bank, Sheffield S10 2TN, UK

Introduction

Matrix population models (MPMs hereafter) are one of the most common mathematical models in ecology, which describe the dynamics of stage-structured populations (Caswell 2001; Salguero-Gómez and de Kroon 2010) as:

$$\mathbf{x}_{t+1} = \mathbf{A}\mathbf{x}_t, \tag{1}$$

where $\mathbf{x}_t$ denotes population vector at time t whose element represents the number of individuals at each stage and $\mathbf{A}$ represents the population projection matrix. Matrix $\mathbf{A}$ includes important life history parameters in their elements, such as survival probability and fecundity, and provides us many population statistics via calculation of linear-algebraic quantities of $\mathbf{A}$, i.e., population growth rate, stable stage distribution, sensitivity, elasticity or life expectancy (Caswell 2001).

Among these, elasticity is a frequently used statistic and given by the relative change in a statistic of the population (e.g., the population growth rate λ) per relative change in matrix elements (Caswell et al. 1984; de Kroon et al. 1986, 2000; van Groenendael et al. 1994; Pfister 1998; Kaneko et al. 1999; Cruz-Rodriguez et al. 2009; Kaneko and Takada 2014; Yokomizo et al. 2017). Because it is calculated based on relative changes, the elasticity of population growth rate to matrix elements is formulated as the limit of the ratio of proportional changes in population growth rate (λ) to that in the matrix elements (a_{ij}):

$$e_{ij} = \lim_{\Delta a_{ij} \to 0} \frac{\Delta\lambda}{\lambda} \Big/ \frac{\Delta a_{ij}}{a_{ij}} = \frac{a_{ij}}{\lambda} \frac{\partial\lambda}{\partial a_{ij}}, \tag{2}$$

where $\Delta\lambda$ and Δa_{ij} denote the changes in λ and a_{ij}, respectively. Therefore, $\Delta\lambda/\lambda$ and $\Delta a_{ij}/a_{ij}$ mean the proportional changes in population growth rate and matrix element. The e_{ij}s are normally presented in matrix form and biologically interpreted as the degree of the relative impact of a demographic process expressed by a_{ij} onto the population growth rate. The elements of any elasticity matrix are proven mathematically to satisfy a conservation law whereby the sum of the elasticities over all the elements is equal to unity: $\sum_i \sum_j e_{ij} = 1$ (de Kroon et al. 1986). This property of the elasticity matrix has been used in multiple inter- and intra-specific demographic analyses in plants (Silvertown et al. 1996).

Silvertown and collaborators published a series of papers applying elasticity analysis to plants to classify their life forms. In these papers, they proposed a scheme of division of the matrix elements into three categories, i.e., fecundity, growth, and stasis (in their case defined as no change in stage [true stasis] as well as retrogression), and defined three types of elasticities of λ: $E_{\text{Fecundity}}$, E_{Growth} and E_{Stasis} (Silvertown and Franco 1993; Silvertown et al. 1993, 1996; Franco and Silvertown 1996, 2004). $E_{\text{Fecundity}}$ is the sum of the elasticities of λ to all fecundity elements in the MPM, and the others are defined similarly. Under these definitions, the sum of the above three elasticities is equal to 1 because of the aforementioned conservation law. Therefore, the elasticity vector $\boldsymbol{E} = (E_{\text{Fecundity}}, E_{\text{Growth}}, E_{\text{Stasis}})$ of any MPM can be plotted on a ternary plot (i.e., two-dimensional simplex in mathematics, Fig. 1a) because the lengths of $E_{\text{Fecundity}}$, E_{Growth}, and E_{Stasis} in Fig. 1a sum up to 1 for any point in the right triangle with side 1 long.

Silvertown et al. (1996) obtained the elasticity vectors for 84 plant species, including trees and herbs, and mapped

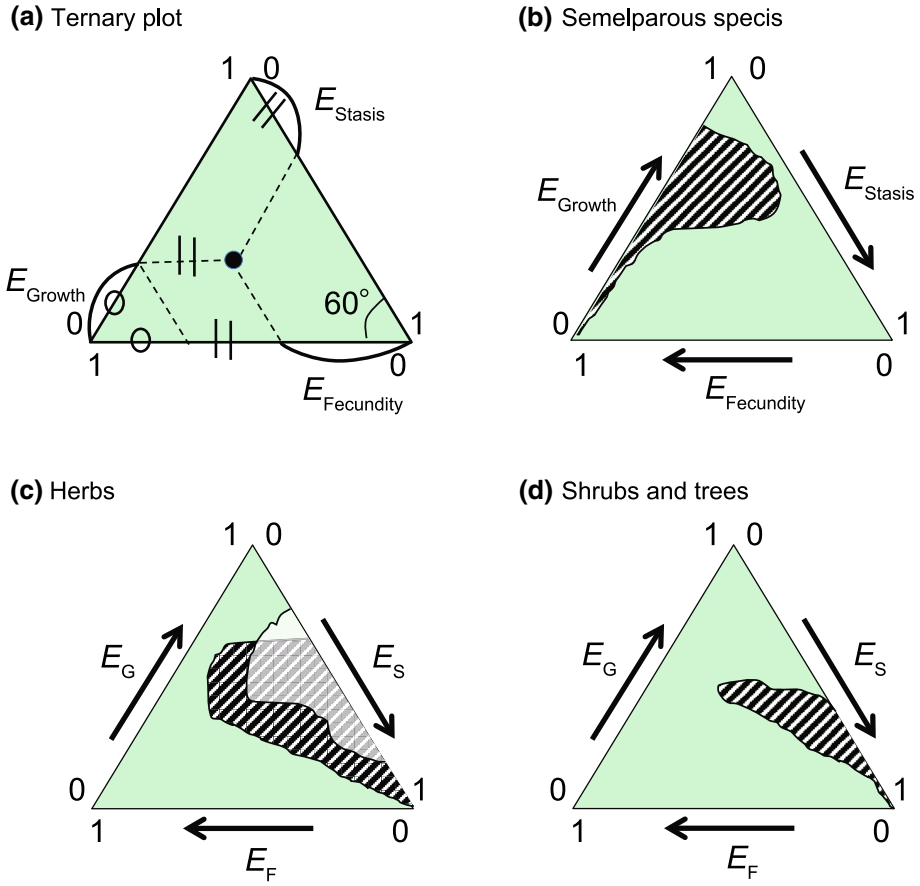

Fig. 1 Ternary plot (=triangle simplex) of the elasticity vector ($\boldsymbol{E}$) for 84 wild plant species' populations. Three elements of the elasticity vector ($\boldsymbol{E}$) are the sum of the elasticities of three main demographic processes: fecundity (F), growth (G) and stasis (S). **a** Coordinates of elasticity vector $\boldsymbol{E} = (E_{\text{Fecundity}}, E_{\text{Growth}}, E_{\text{Stasis}})$ in the ternary plot. $E_{\text{Fecundity}} + E_{\text{Growth}} + E_{\text{Stasis}} = E_{\text{Fecundity}} +$ "o" + "‖" = 1 because of the right triangle; **b** area occupied by semelparous species, **c** by herbs in open habitats (hatched) and in forest habitats (white), and **d** by shrubs and trees. Note that the area occupied by herbs in open habitat overlaps with that in forest habitat. (redrawn from Fig. 2 in Silvertown et al. 1996)

them on a ternary plot. They showed that the location of a species in the ternary plot, as given by its elasticity vector, depended on its life form (or life history). The authors discussed the relationship between the distribution of the species' vectors and the characteristics of their life form (or life history) (Fig. 1b–d). Semelparous species were distributed in the upper-left region of the triangle, where growth and fecundity are more important to λ than stasis (Fig. 1b), whereas herbs occupied a region from the center toward the $E_{\text{Stasis}} = 1$ vertex (Fig. 1c). Importantly, woody species, characterized by slow growth, were found within a relatively narrow strip from the vertex $E_{\text{Stasis}} = 1$ (Fig. 1d).

Two striking patterns were found by plotting the elasticity vectors on the ternary plot. First, few elasticity vectors were located on the lower half area of the triangle, corresponding to species whose λ values would depend strongly on stasis and intermediately to fecundity (Fig. 1). Second, most of the regions spread from the lower right vertex, where the population dynamics are fully dominated by stasis. To understand and clarify the reason for the above two patterns, we constructed four archetypes of population matrices in which the elements were randomly generated from two probability distributions ["randomly generated population matrix" (RPM) hereafter]. We examined the distribution of the elasticity vectors of RPMs and answered the following addressed questions: (1) What is the potential range of space occupied by RPMs in the triangle simplex? (2) Is there any special elasticity distribution in matrices with high population growth rates? (3) Where do the elasticity vectors distribute when we assume a different archetype for the RPMs? (4) Why are the elasticity vectors of natural populations distributed in the upper half of the triangle?

A comparison of the distributions derived from four archetypes reveals the reason behind the characteristic patterns reported by Silvertown et al. (1996). Furthermore, we obtain the elasticity vectors of data from 1230 MPMs (166 plant species) in the COMPADRE database (Salguero-Gómez et al. 2015) and show that there are two straight lines in the distribution of the elasticity vectors from natural populations. Finally, we answer the four aforementioned questions and discuss the applicability of RPMs in evolutionary ecology and perspectives related to this approach.

Methods

Elasticity analysis of life cycle archetypes

We constructed multiple 4×4 RPMs composed of two key demographic processes: fecundity (f) and transition probabilities from a particular stage to another (t_{ij}). The fecundity part was located in only one matrix element, element (1, 4) of the matrix, corresponding to the recruitment into the smallest/least developed/youngest class by reproductive individuals from the largest/most developed/oldest class, as

$$\mathbf{A} = \begin{pmatrix} t_{11} & t_{12} & t_{13} & f \\ t_{21} & t_{22} & t_{23} & t_{24} \\ t_{31} & t_{32} & t_{33} & t_{34} \\ t_{41} & t_{42} & t_{43} & t_{44} \end{pmatrix}. \quad (3)$$

The fecundity (f) was randomly generated using a Poisson distribution with average p:

$$\mathrm{P}(f) = \frac{p^f \exp(-p)}{f!},$$

where P(f) represents the probability that the fecundity is equal to f and f is a non-negative integer. "RandomVariate" command in Mathematica 10 (Wolfram Research, Inc.) was used in generating random samples of fecundity and the generated sequence was, e.g., (4, 2, 4, 8, 8, 7, 9, 6, 3, 5, 7, 7, 2, 5, 3, 7, 6, 4, 6, 7, …) when $p = 5$. We assigned the ith element in the sequence to fecundity in the ith constructed matrix. The Poisson distributions with $p = 5$ and 20 were used in the present paper.

Transition probabilities (t_{ij}) ranged from 0 to 1 and the column sums were constrained to ≤ 1, reflecting the biological requirement that individuals at a given stage cannot survive over 100% between time steps. The probabilities at the jth stage (t_{ij}) were randomly generated using the "RandomReal" command in Mathematica 10, e.g., (0.4459, 0.4955, 0.1836, 0.5721, 0.7747), and the numbers were normalized by dividing them by their sum so that the sum was equal to 1: (0.1804, 0.2005, 0.0743, 0.2314, 0.3134). Then, we assumed the 5-th normalized number (0.3134) was the death probability at the stage and assigned the first four (three when $j = 4$) numbers to t_{1j}, t_{2j}, t_{3j} and t_{4j} (t_{2j}, t_{3j} and t_{4j} when $j = 4$). All the transition probabilities ($j = 1$ to 4) were obtained by four-times iteration of the above procedure. An example of a randomly generated population matrix (RPM) is as follows:

$$\mathbf{A} = \begin{pmatrix} 0.1804 & 0.0150 & 0.2004 & 4 \\ 0.2005 & 0.1944 & 0.3353 & 0.2968 \\ 0.0743 & 0.3687 & 0.2868 & 0.5106 \\ 0.2314 & 0.1057 & 0.1261 & 0.0330 \end{pmatrix}.$$

To explore the elasticity vector distribution in ternary space that can be generated by this type of RPM, we constructed the following four archetypes:

Archetype I: The matrix of this type $\mathbf{A}_1$ has the same form as Eq. 3, where $f > 0, 0 < t_{ij} < 1, \sum_i t_{ij} < 1$. All elements are positive, although they may be very small. This RPM

describes a life history where individuals can progress and retrogress rapidly.

Archetype II: $\mathbf{A}_2$ has the same form as archetype I, i.e., Eq. 3, where $f>0,\ 0<t_{ij}<1,\ \sum_i t_{ij}<1, \sum_i t_{ij}<\sum_i t_{i,j+1}$. Because $\sum_i t_{ij}$ represents the survival probability at the jth stage, the fourth inequality biologically means that the survival probability increases monotonously as the individuals advance to later stages. This RPM, as the one in the first archetype, also allows for rapid progression and retrogression, and is more realistic in that it scales up survival with size/age/stage (e.g., Harper 1977).

$$\text{Archetype III}: \mathbf{A}_3 = \begin{pmatrix} t_{11} & 0 & 0 & f \\ t_{21} & t_{22} & 0 & 0 \\ 0 & t_{32} & t_{33} & 0 \\ 0 & 0 & t_{43} & t_{44} \end{pmatrix}, \tag{4}$$

where $f>0$, $0\le t_{ij}<1$, $\sum_i t_{ij}<1$. We assumed in matrix $\mathbf{A}_3$ that the positive elements are assigned only on element (1, 4) and the diagonal and lower sub-diagonal elements. This RPM represents the life cycle of a species where retrogression is not allowed, and progression can only happen to the immediately larger/more developed stage (slow progression, e.g., trees).

Archetype IV: $\mathbf{A}_4$ has the same general form as archetype III and Eq. 4, where $f>0$, $0\le t_{ij}<1$, $\sum_i t_{ij}<1$. We made the further assumption that $\sum_i t_{ij}<\sum_i t_{i,j+1}$, as in archetype II. Therefore, the two assumptions of archetypes II and III are combined in $\mathbf{A}_4$. This RPM represents a more realistic case than the previous one in that survival increases with size/developmental stage.

We generated 3000 RPMs for each of the four archetypes and $p=5$ and 20 (24,000 matrices), and calculated the elasticities,

$$\begin{pmatrix} e_{11} & e_{12} & e_{13} & e_{14} \\ e_{21} & e_{22} & e_{23} & e_{24} \\ e_{31} & e_{32} & e_{33} & e_{34} \\ e_{41} & e_{42} & e_{43} & e_{44} \end{pmatrix}, \tag{5}$$

using the formula of elasticity (Caswell 2001):

$$e_{ij} = \frac{v_i u_j}{\sum_k v_k u_k}, \tag{6}$$

where v_i (or u_j) represents the ith (or the jth) element of the left (or right) eigenvector of each RPM. These 16 elasticities were summarized to a vector $\boldsymbol{E} = (E_{\text{Fecundity}}, E_{\text{Growth}}, E_{\text{Stasis}})$ following a way that Silvertown et al. (1996) assumed: assigning element (1, 4) to the fecundity category (F), the diagonal elements and retrogression elements to the stasis category (S), and the lower triangle elements to the growth category (G), i.e.,

$$\begin{pmatrix} S & S & S & F \\ G & S & S & S \\ G & G & S & S \\ G & G & G & S \end{pmatrix}. \tag{7}$$

Therefore,

$$\begin{aligned} E_{\text{Fecundity}} &= e_{14} \\ E_{\text{Growth}} &= e_{21}+e_{31}+e_{32}+e_{41}+e_{42}+e_{43} \\ E_{\text{Stasis}} &= e_{11}+e_{12}+e_{13}+e_{22}+e_{23}+e_{24}+e_{33}+e_{34}+e_{44} \end{aligned} \tag{8}$$

The 3000 points of elasticity vectors $\boldsymbol{E}$ of the RPMs were plotted and distributed in a ternary plot (two-dimensional plane), as described in Fig. 1. Eight distributions of the vectors were obtained in all ($p=5$ and 20 in archetype $\mathbf{A}_1$; $p=5$ and 20 in archetype $\mathbf{A}_2$; $p=5$ and 20 in archetype $\mathbf{A}_3$; $p=5$ and 20 in archetype $\mathbf{A}_4$).

We obtained several statistics of elasticity vector distribution to estimate the effect of the population growth rate (Table 1a), levels of reproduction (p; Table 1b) and archetype (Table 1c) on the distributions. The statistics are the mean and the standard deviation of each distribution and Sørenson distance index between two distributions, which were used to compare two distributions. The means were used to estimate how much the center of the distribution shifts between the two distributions. Sørenson distance index (S_{index}) is a measure used to estimate the degree of overlap of two distributions. To calculate S_{index}'s, we made a polygon for each elasticity vector distribution, which is a region including all the distributed points inside the closed curve, as shown in Fig. 2a. Then, two polygons were obtained from two elasticity vector distributions to be compared (Fig. 2b) and S_{index} of the two polygons was calculated using the definition of $2x/(2x+y+z)$, where x, y and z represent the overlap area of the first and the second polygons, the area unique to the first polygon and the area unique to the second polygon, respectively (Fig. 2b). It is equal to 1 when two areas are the same ($y=z=0$) and equal to zero when they are not overlapped. S_{index} can be used to estimate how much the whole distributions differ. The comparison was made in three ways as follows: between the distributions for $\lambda>1$ vs. $\lambda<1$, between the distributions for $p=5$ vs. 20 in each archetype, and between the distributions of archetypes I vs. II.

Furthermore, we obtained a mathematical formula on the elasticity vectors analytically in archetypes III and IV and proved mathematically that the distribution should lie on a line. We also obtained a formula to determine the angle (θ) of the straight line [see Electronic Supplementary Material (ESM) S1].

Table 1 The comparisons among elasticity vector distributions

	Population growth rate	Mean	SD	Sørenson index (%)	Figures
(a) Comparison between the distributions for $\lambda > 1$ and $\lambda < 1$					
Archetype I ($p = 5$)	$\lambda > 1$	{0.312, 0.469, 0.219}	{0.060, 0.036, 0.071}	46.3	Figure 3a
	$\lambda < 1$	{0.161, 0.422, 0.417}	{0.070, 0.058, 0.114}		
Archetype II ($p = 5$)	$\lambda > 1$	{0.291, 0.458, 0.251}	{0.062, 0.039, 0.073}	46.2	Figure 3c
	$\lambda < 1$	{0.149, 0.409, 0.442}	{0.062, 0.057, 0.101}		
Archetype III ($p = 5$)	$\lambda > 1$	{0.141, 0.424, 0.435}	{0.035, 0.105, 0.141}	93.5	Figure 3e
	$\lambda < 1$	{0.118, 0.356, 0.526}	{0.047, 0.142, 0.190}		
Archetype III ($p = 20$)	$\lambda > 1$	{0.164, 0.490, 0.346}	{0.031, 0.094, 0.126}	90.8	Figure 3f
	$\lambda < 1$	{0.128, 0.385, 0.487}	{0.045, 0.134, 0.178}		
Archetype IV ($p = 5$)	$\lambda > 1$	{0.109, 0.328, 0.563}	{0.030, 0.089, 0.119}	97.1	Figure 3g
	$\lambda < 1$	{0.065, 0.194, 0.741}	{0.039, 0.116, 0.155}		
Archetype IV ($p = 20$)	$\lambda > 1$	{0.138, 0.415, 0.447}	{0.029, 0.087, 0.116}	82.8	Figure 3h
	$\lambda < 1$	{0.079, 0.237, 0.684}	{0.040, 0.121, 0.162}		

	Mean	SD	Sørenson index (%)	Figures
(b) Comparison between the distributions for $p = 5$ and 20 in each archetype.				
Archetype I ($p = 5$)	{0.304, 0.466, 0.230}	{0.070, 0.040, 0.087}	62.0	Figure 3a
($p = 20$)	{0.389, 0.496, 0.115}	{0.055, 0.031, 0.051}		Figure 3b
Archetype II ($p = 5$)	{0.279, 0.453, 0.268}	{0.074, 0.044, 0.093}	55.3	Figure 3c
($p = 20$)	{0.373, 0.489, 0.138}	{0.059, 0.034, 0.054}		Figure 3d
Archetype III ($p = 5$)	{0.130, 0.388, 0.482}	{0.044, 0.131, 0.174}	96.1	Figure 3e
($p = 20$)	{0.157, 0.472, 0.371}	{0.037, 0.110, 0.146}		Figure 3f
Archetype IV ($p = 5$)	{0.096, 0.288, 0.617}	{0.039, 0.116, 0.114}	91.7	Figure 3g
($p = 20$)	{0.132, 0.397, 0.471}	{0.035, 0.106, 0.141}		Figure 3h

	Mean	SD	Sørenson index (%)	Figure
(c) Comparison between the distributions of archetypes I and II				
Archetype I ($p = 5$)	{0.304, 0.466, 0.230}	{0.070, 0.040, 0.087}	91.3	Figure 3a
Archetype II	{0.279, 0.453, 0.268}	{0.074, 0.044, 0.093}		Figure 3c
Archetype I ($p = 20$)	{0.389, 0.496, 0.115}	{0.055, 0.031, 0.051}	93.9	Figure 3b
Archetype II	{0.373, 0.489, 0.138}	{0.059, 0.034, 0.054}		Figure 3d

The mean and SD of the elasticity vectors are shown as the statistics of each distribution and Sørenson distance indices of two distributions are calculated to estimate the degree of overlapping
In archetypes III and IV, we calculated the overlapping length of two straight lines as a one-dimensional Sørenson distance index

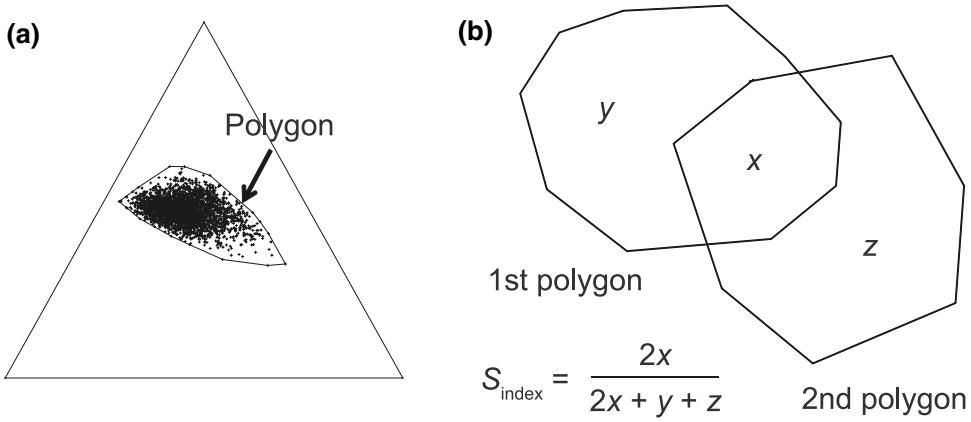

Fig. 2 Polygon and Sørenson distance index. **a** A polygon can be drawn for an elasticity vector distribution, which has 3000 points (small "+" marks). It is a region including all the distributed points inside the closed curve. **b** Two polygons obtained from two elasticity vector distributions are composed of three areas: the overlap area of the first and second polygons, the area unique to the first polygon and the area unique to the second polygon. Their areas are *x, y* and *z*, respectively. Sørenson distance index (S_{index}) is calculated as $2x/(2x+y+z)$

Elasticity analysis of natural populations

We sampled MPMs from the COMPADRE Plant Matrix Database (Salguero-Gómez et al. 2015) to obtain the elasticity vectors. COMPADRE (ver. 4.0.1) contains 4246 "individual" MPMs from 695 plant species. Each individual MPM describes the dynamics of a given population at a single site and study time step for a given treatment. To retain MPMs of the highest quality, we applied a series of selection criteria: (a) only MPMs where the estimated stage-specific survival rates are ≤ 1.; (b) populations where fecundity is explicitly measured; (c) populations parameterized as "unmanipulated" treatment conditions (i.e., controls), (d) MPMs with a sampling periodicity = 1, which means that the time step in calculating the population dynamics is 1 year to allow for cross-taxonomic comparisons of perturbation of λ on the same basis; and (e) MPMs that are irreducible and primitive to be able to calculate elasticities. In biological terms, a reducible matrix means that the life cycle contains at least one stage that cannot contribute, by any developmental path, to some other stage(s). Otherwise, the matrix is irreducible (Caswell 2001). In primitive matrices, the stable stage distribution is realized in the long-term dynamics and periodical behavior of the dynamics does not exist (Caswell 2001). This criterion ensures that the elements of the sensitivity matrix are all positive; (f) MPMs with seed stages were excluded because of the considerable uncertainty in their parameter estimation in field conditions, as the inclusion of a seed stage can result in an artifactual year gap (Caswell 2001; Salguero-Gómez et al. 2015). For criterion (d), the irreducibility of each MPM was checked by examining whether $(\mathbf{I}+\mathbf{A})^{n-1}$ results in a positive matrix using a theorem proposed by Horn and Johnson (1985). n and $\mathbf{I}$ in the equation represent the matrix dimension of $\mathbf{A}$ and the identity matrix, respectively. The primitivity of a given MPM was checked by examining whether or not $\mathbf{A}^{n^2-2n+2}$ is a positive matrix.

Our set of selection criteria applied to COMPADRE resulted in 1230 MPMs from 166 plant species. The elasticity vectors of these MPMs were plotted in the triangle simplex, as were those generated from the RPMs, which then allowed us to examine the full space of elasticity vectors that can be explored by a RPM vs. those found in nature.

Results

Elasticity analysis of life cycle archetypes

Figure 3 shows the distributions of elasticity vectors of the RPMs on the ternary plot space in each archetype with a low or high fecundity parameter. In archetype I, representing a life cycle where only 4th stage individuals can reproduce and where individuals can progress and retrogress rapidly but without a relationship between survival and stage number, the distribution of elasticity vectors was concentrated in the upper-center region of the ternary plot (Fig. 3a, b); thus, differing from the overall result reported by Silvertown et al. (1996; Fig. 1). Specifically, our distribution shifted to the upper-left region (i.e., greater importance for fecundity and growth to λ, lower for stasis) when we increased the fecundity parameter from $p = 5$ to 20 (Fig. 3b; Table 1b). The overlapping index by Sørenson of the distributions in Fig. 3a, b is 62.0%. The average fecundity affected the number of points resulting in values of λ above or below. This is due to the fact that increasing fecundity leads to more recruits in the population. Additionally, the classification

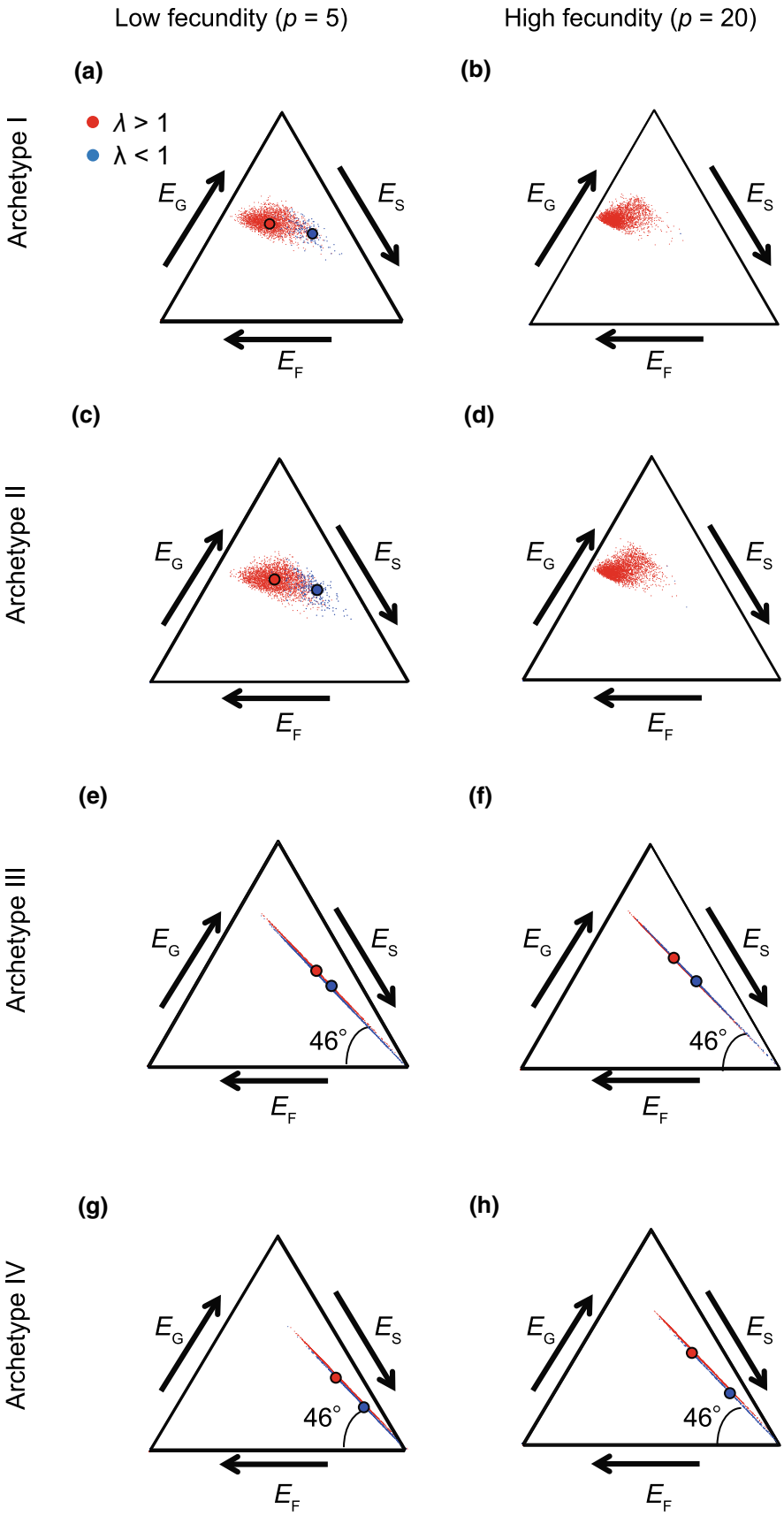

Fig. 3 Ternary plot of the elasticity vector ($\boldsymbol{E}$) for 3000 simulated 4-stage matrix population models. $\boldsymbol{E} = (E_{\text{Fecundity}}, E_{\text{Growth}}, E_{\text{Stasis}})$. The elasticity vector distribution is shown in each of the four inspected archetype life cycles: archetype I: rapid progression and retrogression are allowed (See Eq. 3); archetype II: same as archetype I, but survival increases with stage number; archetype III: retrogression does not occur, and progression can only occur to the immediately superior class, mimicking the demography of slow-living creatures, such as trees; archetype IV: same as III, but survival increases with stage number. Blue (red) dots correspond to simulated models where the emerging is <1 (>1). The blue (red) dot with solid line represents the mean of elasticity vector for <1 (>1). Ternary plots are presented for two levels of reproduction: $p=5$ (left) and $p=20$ (right). Note that, for archetypes III and IV, the distribution on the triangle simplex spreads along a straight line departing from $E_S = 1$ with an angle $\theta=46°$

of RPMs into two groups, depending on whether $\lambda >$ or < 1, provides another useful insight: the distributions of archetypes I moved toward the lower-right region when $\lambda < 1$ and the overlap between the $\lambda > 1$ distribution and the $\lambda < 1$ distribution is 46.3% (Fig. 3a; Table 1a).

Archetype II occupied a similar area to archetype I. In archetype II, simulated RPMs followed the same assumptions as in archetype I, but in them, survival probabilities increased with stage development. The resulting distributions are shown in Fig. 3c, d and the distribution shifted to the upper-left region when we increased the average fecundity ($p = 20$; Fig. 3d). The overlap of the distributions in Fig. 3c, d is 55.3% as shown in Table 1b. Additionally, the classification of RPMs into $\lambda > 1$ and $\lambda < 1$ groups affected the distributions of archetypes II, shifting towards the lower-right region when $\lambda < 1$ .The overlap between the $\lambda > 1$ distribution and the $\lambda < 1$ distribution is 46.2% (Fig. 3c; Table 1a).

From the comparison between archetypes I and II, the mean of the distribution tended slightly (not large) toward an area of relatively greater impact by stasis (bottom-right corner) compared with the area occupied by archetype I (Table 1c). The overlap area in archetypes I and II is high, as depicted by a Sørenson index of 91.3% ($p = 5$) and 93.9% ($p = 20$) between both distributions.

The distributions of the elasticity vectors of archetype III and IV are strikingly different from those by archetypes I and II. The main difference of the assumption between both sets of archetypes is that in III and IV, individuals were not allowed to retrogress, nor to progress further than to its immediately superior stage (e.g., rapid progression was not possible; Eq. 4). The elasticity vectors in archetypes III and IV produced a straight line departing from the lower-right corner, where the relative impact of stasis on λ is the highest possible ($E_{\text{Stasis}} = 1$), and at $\theta = 46°$ (Fig. 3e–h). Comparing the distributions in archetype III depending on whether $\lambda >$ or < 1, the two distributions were found to be similar irrespective of fecundity parameter value (Fig. 3e, f). The line moved slightly to the lower-right corner when λ was less than 1. The overlap as per Sørenson index was high: 93.5% ($p = 5$) and 90.8% ($p = 20$) (Table 1a). It should be noted that we calculated the overlapping length of two straight lines as a one-dimensional Sørenson distance index. The distribution in archetype IV had a similar tendency as that of archetype III (Fig. 3g, h; Table 1a, b). Moreover, the spread of the line was greater for archetype III than for archetype IV; the length of the respective distributions was 0.813 and 0.672 (Fig. 3e, g), and 0.845 and 0.726 (Fig. 3f, h).

Given the striking linear pattern of archetypes III and IV, we obtained a formula on the elasticity vectors analytically:

$$E_{\text{Fecundity}} = \frac{1}{D\lambda}, \quad E_{\text{Growth}} = \frac{(n-1)}{D\lambda} \text{ and } E_{\text{Stasis}} = 1 - \frac{n}{D\lambda}, \tag{9}$$

where n is the matrix dimension and $D = \sum_k \frac{1}{\lambda - t_{kk}}$. Note that the elasticity of growth element $(i+1, i)$ is $e_{i+1,i} = \frac{1}{D\lambda}$ and independent of i, which means all the values are the same and are the same as $E_{\text{fecundity}}$ (see ESM S1). Because the elements of the elasticity vector depend on only one term, λ, the degree of freedom of elasticity vectors is 1. Therefore, the elasticity vector distribution lies on a straight line, varying the value of $D\lambda$. Eliminating $D\lambda$ from Eq. 9, a formula to determine the angle (θ) of the straight line can be obtained as

$$\tan\theta = \frac{(n-1)\sqrt{3}}{(n+1)}. \tag{10}$$

We note that in all four archetypes examined here, the number of stages in the life cycles were 4, thus $n = 4$, and $\tan 46° = 3\sqrt{3}/5$.

Furthermore, to confirm the above results, we conducted the same simulations taking a different approach to construct randomly generated population matrices. The results of the additional simulations are similar to the results in this subsection (see ESM S2).

Elasticity analysis of natural populations

The elasticity vectors of the 1230 MPMs selected from the COMPADRE database represent the relative importance of the demographic processes for each species under natural conditions, and the covariance of vital rates that incorporates biological trade-offs among those functions. Keeping these natural restrictions in mind, one can observe that the elasticity vectors of these natural populations lay mostly in the upper half of the triangle simplex (Fig. 4a). This means that most of the examined populations are relatively dominated by growth and stasis (with retrogression, see Eq. 7), but not as much by fecundity. Furthermore, we found two straight lines departing from the lower-right region running towards the center of the ternary space, with slopes of 30° and 41°, respectively (Fig. 4b). These angles are given from Eq. 10, and correspond to matrix dimensions of 2 and 3:

$$\tan 30° = \frac{(2-1)\sqrt{3}}{(2+1)} = \frac{\sqrt{3}}{3} \quad \text{and} \quad \tan 41° = \frac{(3-1)\sqrt{3}}{(3+1)} = \frac{\sqrt{3}}{2}.$$

We examined how many MPMs from the selected 1230 matrices had the same form as Eq. 4, i.e., a single fecundity element and diagonal and lower sub-diagonal elements are not equal to zero. There were 412 matrices, including 332 two-by-two MPMs and 33 three-by-three MPMs (Table 2). The elasticity vector of 33.5% of 1230 MPMs fell on these straight lines. Note that all two-by-two matrices have the same form as Eq. 3.

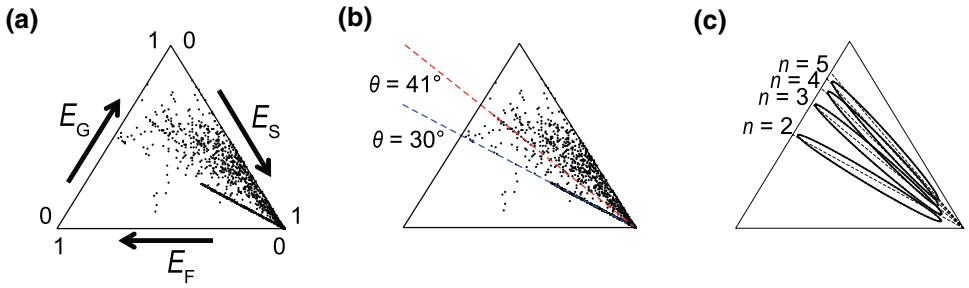

Fig. 4 Ternary plot of the elasticity vector ($\boldsymbol{E}$) for 1230 matrix population models (MPMs) from 166 plant species in the COMPADRE database. $\boldsymbol{E} = (E_{\text{Fecundity}}, E_{\text{Growth}}, E_{\text{Stasis}})$. Two straight lines can be observed: one in the lower-right region and another in the center of the ternary plot. The slopes of these lines correspond to matrix dimensions 2 and 3, as per Eq. 10. **a** Original distribution of the examined species from COMPADRE. **b** Two dashed lines with slopes of 30° (blue) and 41° (red) are added to **a. c** Conceptual panel showing five straight lines and scattered distributions around each line for a given matrix dimension n, ranging from two to five

Table 2 The numbers of matrix population models (MPMs) that have the same form as Eq. 4

Matrix dimension	Number of matrices
2	332
3	33
4	1
5	37
6	2
7	3
8	0
9	4
Total	412

412 matrices are selected in 1230 MPMs from the COMPADRE dataset

Discussion

We obtained the elasticity vectors ($E_{\text{Fecundity}}, E_{\text{Growth}}, E_{\text{Stasis}}$) from four archetypes of RPMs to compare them to those obtained and represented these elasticity vectors in a ternary plot from the MPMs of 84 plant species in Silvertown et al. (1996), where an effort was made to explain the main drivers behind the location of species on the ternary plot. We next validated our results with an unprecedented number of MPMs from natural populations worldwide to answer questions (1)–(4) in the "Introduction", also detailed below:

What is the potential range of space occupied by RPMs in the triangle simplex?

The distribution of the elasticity vectors in RPMs of $\mathbf{A}_1$ (archetype I) was located in the upper-center region and discorded from the distributions of elasticity vectors of any life forms analyzed by Silvertown et al. (1996). In Fig. 3a, b, our distribution was mostly concentrated in a sparse region of the distribution found by Silvertown and his collaborators and dominated by growth (Fig. 1). This discrepancy is expected because RPMs of archetype I were constructed only considering minimum biological assumptions and/or requirements, such as non-negative matrix elements and the column sums being less than 1. To understand the reason for the discrepancy, one of the plausible biological requirements could be that more developed individuals do tend to survive better because they may be more tolerant to environmental stresses and/or may be better competitors (Harper 1977). However, when we explicitly considered this biological requirement, as we did in archetype II, we still found a similar result to that of archetype I (Fig. 3c, d). Therefore, we conclude that the difference in assumptions between archetypes I and II is not the main reason for the difference between the distributions reported here and those in Silvertown et al. (1996; Fig. 1).

Is there any special elasticity distribution in matrices with high population growth rates?

Our approach, i.e., producing RPMs constrained to a series of assumptions, can be thought of as a simulation exercise where mutations enter a specific population. Most of the mutations would be driven out in the process of natural selection because the fitness is less than 1. Successful mutations alter the fitness of the individuals therein, and consequently the overall population growth rate. The mutations would then determine where species are located on the ternary plot, and what optimal relationships of investments on fecundity, growth and stasis are optimal for natural selection. Ultimately, the essential cause of being favored by natural selection is that the population-average fitness (i.e.,) is more than 1 (Takada 1995; Chap. 11 in Caswell 2001; Geyer et al. 2007). Where are the elasticity vectors that correspond to RPMs with $\lambda > 1$ located in the ternary plot? We found some general support to a unique answer in addressing this question. The elasticity

vector distribution of RPMs moved to the upper-left region of the ternary plot when the population growth rate was greater than 1 in both Fig. 3a, c. Furthermore, the distribution of elasticity vectors migrated to the upper-left region of the ternary plot, with an increased impact of fecundity on the population growth rate, when comparing Fig. 3a, b (c, d). This means that both the relative impacts of fecundity and growth to the overall population dynamics increase with an increase in fecundity. The same tendency was evidenced by our results in Fig. 3e–h. However, the distribution of elasticity vectors of plants from natural settings in Silvertown et al. (1996) and COMPADRE rarely occupies the upper-left region (Figs. 1, 4a). Instead, these are located in the lower-right region. Before we conducted the simulated calculation on RPMs, we expected that some evolutionary force must operate for the bias in elasticity distribution of natural plant populations. The first candidate of the evolutionary force we considered was population viability; whether the population growth rate is greater than 1 or not. However, the viability shifted the distribution toward the upper-left region, which is the opposite side of the distribution in natural populations. Therefore, the viability in plant populations is not the reason for interpreting the elasticity distribution of real plants.

Where do the elasticity vectors distribute when we assume different archetypes of RPMs?

Under the assumption that most plants in nature do not grow fast, as it happens in trees (Hartshorn 1975; Platt et al. 1988; van Mantgem and Stephenson 2005; Lin and Augspurger 2008; Münzbergová et al. 2013; Salguero-Gómez et al. 2016), i.e., the RPMs given by Eq. 4, the elasticity distribution lies along a line with a slope of 46° (Fig. 3e, f). The region of elasticity vectors had a similar distribution to that of woodland herbs, shrubs, and trees (Fig. 1c, d). We have proven mathematically here that matrices with the special structure of Eq. 4 result in a linear distribution of elasticity vectors (see ESM S1). Not coincidentally, two straight lines were found in the triangle map obtained from the population matrices of COMPADRE (Fig. 4), which explained 35.1% of the 1230 plant species (432 species). If the assumption that most plants do not grow quickly is "approximately" correct in the remaining 64.9% of plants, the distribution of elasticity vectors would be scattered around a straight line depending on the matrix dimension n (see Eq. 10). Therefore, the distributions in Figs. 1 and 4a could be the assemblage of several distributions around several straight lines (Fig. 4c). We speculate that the special structure of projection matrices, i.e., the assumption of not growing quickly, is one of the important reasons for the observed elasticity distribution. It will be an interesting subject to explore whether the assumption "approximately" holds in the remaining 64.9% of plants.

Why are the elasticity vectors of natural populations distributed in the upper half of the triangle?

The slope of the linear distribution of elasticity vectors depends on the dimension of the projection matrix, as in Eq. 10. When the dimension is 2, the slope is 30° (Fig. 4b). As n approaches ∞,

$$\tan\theta = \lim_{n\to\infty} \frac{(n-1)\sqrt{3}}{(n+1)} = \sqrt{3},$$

and the angle tends to 60°. Therefore, the elasticity distribution obtained from projection matrices with a variety of matrix dimensions would be distributed between lines with slopes of 30° and 60° (Fig. 4c). Therefore, most of the elasticity vectors of natural populations would be distributed in the upper half of the triangle.

When validating our simulations with MPMs from COMPADRE, which were carefully chosen to represent natural settings under control conditions, we found that there were two straight lines in the ternary plot. The result clarified that the distribution of elasticity vectors strongly depends on matrix dimension and structure (e.g., how many and where zero elements are positioned in the MPM in question and into which stages newly-born offspring are recruited). Therefore, we call for more cautious interpretation of ternary plots of elasticity, specifically in regards to slow-living creatures such as trees, or to age-based MPMs. It is mathematically proven that the elasticity distribution in age-based MPMs lies along a straight line in a ternary plot [see ESM S1 (iii)]. Furthermore, in a comparative study using the matrix database, we should take care in determining selection criteria for appropriate matrices, although the selection criteria depend on the purpose of each study. Specifically, species with clonal reproduction occasionally show a diverse matrix structure, i.e., the newly born individuals created through clonal reproduction are recruited into a variety of stages. Additionally, attention should be paid to the variation in matrix dimensions of MPMs when we use the ternary plot in comparing multiple species.

Several authors have pointed out that the matrix dimension affects the results of demographic statistics such as population growth rates and elasticities (Silvertown et al. 1993; Enright et al. 1995; Lamar and McGraw 2005; Ramula and Lehtila 2005; Salguero-Gómez and Casper 2010; Salguero-Gómez and Plotkin 2010; Yokomizo et al. 2017). If the structure had the form in Eq. 4, the variation in elasticity vectors would occur along a line from the lower-right corner to the edge of the E_{Growth} axis in the upper half of the triangle simplex. Where along this line is the elasticity vector located for a specific demography? This question concerns the very evolution of a plant's life history, and remains unsolved theoretically. We expect this would be an interesting subject to be solved in future.

Acknowledgements We sincerely thank Dr. Motohide Seki, Hiroyuki Yokomizo, Keiichi Fukaya and Yuya Tachiki for their valuable suggestions. We thank the Max Planck Institute for Demographic Research for the development and curation of the COMPADRE Plant Matrix Database. TT was supported in part by JSPS KAKENHI (Grant Numbers JP26291087 and JP15H04418). RSG was supported by the Australian Research Council (DE140100505) and the UK NERC (R/142195-11-1).

References

Caswell H (2001) Matrix population models: construction, analysis and interpretation, 2nd edn. Sinauer Associates, Sunderland

Caswell H, Naiman R, Morin R (1984) Evaluating the consequences of reproduction in complex salmonid life cycles. Aquaculture 43:123–143

Cruz-Rodriguez JA, Lopez-Mata L, Varverde T (2009) A comparison of traditional elasticity and variance-standardized perturbation analyses: a case study with the tropical tree species *Manilkara zapota* (Sapotaceae). J Trop Ecol 25:135–146

de Kroon H, Plaisier A, van Groenendael J, Caswell H (1986) Elasticity: the relative contribution of demographic parameters to population growth rate. Ecology 67:1427–1431

de Kroon H, van Groenendael J, Ehrlén J (2000) Elasticities: a review of methods and model limitations. Ecology 81:607–618

Enright NJ, Franco M, Silvertown J (1995) Comparing plant life histories using elasticity analysis: the importance of life span and the number of life cycle stages. Oecologia 104:79–84

Franco M, Silvertown J (1996) Life history variation in plants: an exploration of the fast–slow continuum hypothesis. Philos Trans R Soc Lond B 351:1341–1348

Franco M, Silvertown J (2004) A comparative demography of plants based upon elasticities of vital rates. Ecology 85:531–538

Geyer CJ, Wagenius S, Shaw RG (2007) Aster models for life history analysis. Biometrika 94:415–426

Harper JL (1977) Population biology of plants. Academic Press, New York

Hartshorn GS (1975) A matrix model of tree population dynamics. In: Golley FB, Medina E (eds) Tropical ecological systems. Springer, New York, pp 41–51

Horn R, Johnson C (1985) Matrix algebra. Cambridge University, Cambridge

Kaneko Y, Takada T (2014) Pair-wise analyses of the effects of demographic processes, vital rates, and life stages on the spatiotemporal variation in the population dynamics of the riparian tree *Aesculus turbinata* Blume. Pop Ecol 56:161–173

Kaneko Y, Takada T, Kawano S (1999) Population biology of *Aesculus turbinata* Blume: a demographic analysis using transition matrices on a natural population along a riparian environmental gradient. Plant Species Biol 14:47–68

Lamar WR, McGraw JB (2005) Evaluating the use of remotely sensed data in matrix population modeling for eastern hemlock (*Tsuga canadensis* L.). For Ecol Manag 212:50–64

Lin Y, Augspurger CK (2008) Impact of spatial heterogeneity of neighborhoods on long-term population dynamics of sugar maple (*Acer saccharum*). For Ecol Manag 255:3589–3596

Münzbergová Z, Hadincová V, Wild J, Kindlmannová J (2013) Variability in the contribution of different life stages to population growth as a key factor in the invasion success of *Pinus strobus*. Plos One 8:e56953

Pfister CA (1998) Patterns of variance in stage-structured populations: evolutionary predictions and ecological implications. Proc Natl Acad Sci USA 95:213–218

Platt WJ, Evans GW, Rathbun S (1988) The population dynamics of a long-lived conifer (*Pinus palustris*). Am Nat 131:491–525

Ramula S, Lehtila K (2005) Matrix dimensionality in demographic analysis of plants: when to use smaller matrices? Oikos 111:563–573

Salguero-Gómez R, Casper BB (2010) Keeping shrinkage in the demographic loop. J Ecol 98:312–323

Salguero-Gómez R, de Kroon H (2010) Matrix projection models meet variation in the real world. J Ecol 98:250–254

Salguero-Gómez R, Plotkin JB (2010) Matrix dimensions bias demographic inferences: implications for comparative plant demography. Am Nat 176:710–722

Salguero-Gómez R, Jones OR, Archer CR, Buckley YM, Che-Castaldo J, Caswell H, Hodgson D, Scheuerlein A, Conde DA, Brinks E, de Buhr H, Farack C, Gottschalk F, Hartmann A, Henning A, Hoppe G, Römer G, Runge J, Ruoff T, Wille J, Zeh S, Davison R, Viergegg D, Baudisch A, Altwegg R, Colchero F, Dong M, de Kroon H, Lebreton JD, Metcalf CJE, Neel MM, Parker IM, Takada T, Valverde T, Vélez-Espino LA, Wardle GM, Franco M, Vaupel JW (2015) The COMPADRE plant matrix database: an open online repository for plant demography. J Ecol 103:202–218

Salguero-Gómez R, Jones OR, Jongejans E, Blomberg SP, Hodgson DJ, Mbeau-Ache C, Zuidema PA, de Kroon H, Buckley YM (2016) Fast–slow continuum and reproductive strategies structure plant life-history variation worldwide. Proc Natl Acad Sci USA 113:230–235

Silvertown J, Franco M (1993) Plant demography and habitat: a comparative approach. Plant Species Biol 8:67–73

Silvertown J, Franco M, Pisanty I, Mendoza A (1993) Comparative plant demography–relative importance of life-cycle components to the finite rate of increase in woody and herbaceous perennials. J Ecol 81:465–476

Silvertown J, Franco M, Menges E (1996) Interpretation of elasticity matrices as an aid to the management of plant populations for conservation. Conserv Biol 10:591–597

Takada T (1995) Evolution of semelparous and iteroparous perennial plants: comparison between the density-independent and density-dependent dynamics. J Theor Biol 173:51–60

van Mantgem PJ, Stephenson NL (2005) The accuracy of matrix population model projections for coniferous trees in the Sierra Nevada, California. J Ecol 93:737–747

van Groenendael J, de Kroon H, Kalisz S, Tuljapurkar S (1994) Loop analysis: evaluating life history pathways in population projection matrices. Ecology 75:2410–2415

Yokomizo H, Takada T, Fukaya K, Lambrinos JG (2017) The influence of time since introduction on the population growth of introduced species and the consequences for management. Popul Ecol 59:89–97